On Climatological Monthly Mean Wind Stress and Wind Stress Curl Fields over the World Ocean*

D. E. HARRISON

Pacific Marine Environmental Laboratory, National Oceanic and Atmospheric Administration, Seattle, Washington

(Manuscript received 6 January 1988, in final form 30 July 1988)

ABSTRACT

Using a version of the global surface marine observation historical data set, a new 1° spatial resolution global ocean surface wind stress climatology has been evaluated using the Large and Pond surface drag coefficient formulation. These new results are compared, after spatial smoothing, with those of Hellerman and Rosenstein, who used a different drag coefficient form. It is found that the new stresses are almost everywhere smaller than those of Hellerman and Rosenstein, often by 20%–30%, which is greater than the formal error estimates from their calculations. The stress differences show large-scale spatial structure, as would be expected given the spatial variation of the surface stability parameter and the known different wind variability regions. Basin zonally averaged Ekman transports are computed to provide perspective on the significance of the stress differences; annual mean differences can exceed 10 Sv (Sv $\equiv 10^6$ m^3 s^{-1}) equatorward of 20° lat, but are smaller poleward. Wind stress curl and Sverdrup transport calculations provide a different perspective on the differences; particularly noticeable differences are found in the regions of the Gulf Stream and Kuroshio separation. Large annual variations in midlatitude wind stress curl suggest that study of the forced response at annual periods should be of interest.

1. Introduction

The low-frequency circulation of the world ocean is forced primarily by the freshwater, momentum, and heat fluxes at its surface. Of these fluxes, the most studied is the momentum flux associated with the stress of the wind on the surface. It is also (arguably) the most important forcing for upper ocean circulation; all large scale basin ocean circulation theories and models begin with at least a specification of the surface stress and/or curl of the stress. It is assumed that the reader is familiar with the basic concepts of ocean flow forced by wind stress and curl (e.g., Ekman and Sverdrup dynamics); see Pedlosky (1979) or Veronis (1973) for reviews of these and other basic concepts.

Wind stress fields have been estimated in many ways over the years. The standard large-scale analysis was, for much of the last two decades, the wind rose–based study of Hellerman (1967). Evanson and Veronis (1975) also made an effort to provide data needed for Veronis' world ocean circulation studies (Veronis 1978 and references therein). Bunker provided another study, in support of studies of water mass formation in the Atlantic; the North Atlantic fields were discussed by Leetmaa and Bunker (1978) and atlases of all the fluxes computed are now being issued (e.g., Isemer and Hasse, 1988). Wyrtki and Meyers (1976) carried out now classic climatological stress calculations for the tropical Pacific; Hastenrath and Lamb (1977, 1979) have done similarly for the tropical Indian and Atlantic Oceans.

Hellerman and Rosenstein (1983; hereafter H&R) have recently published global estimates, using the surface marine dataset, assembled by various national agencies over the past decade, and assuming drag coefficients very similar in form to those used by Bunker (1976). They also made formal error estimates for their fields, based on the number of data and their estimated variances and covariances. These estimates are shown for January and July zonal wind stress in Fig. 1. For January, H&R estimated the standard error to be less than 0.1 dyne cm^{-2} between ~30°S and 35°N in the Atlantic, over most of the Indian Ocean north of 30°S, and in parts of the midlatitude and tropical Pacific; the estimated errors rise sharply poleward of 30°S and ~40°N, to more than 0.25 dyn cm^{-2}. In July, the estimated error is less than 0.1 dyn cm^{-2} north of ~10°S, almost everywhere, and it is >0.25 dyn cm^{-2} south of ~35°S almost everywhere. Maximum error estimates are not given.

Uncertainty in climatological stress estimates comes from unsampled wind variations, from error in the individual observations, from the formula assumed to

* Contribution No. 905 from NOAA/Pacific Marine Environmental Laboratory.

Corresponding author address: Dr. D. E. Harrison, Pacific Marine Environmental Laboratory, NOAA Building Number 3, 7600 Sand Point Way NE, Seattle, WA 98115.

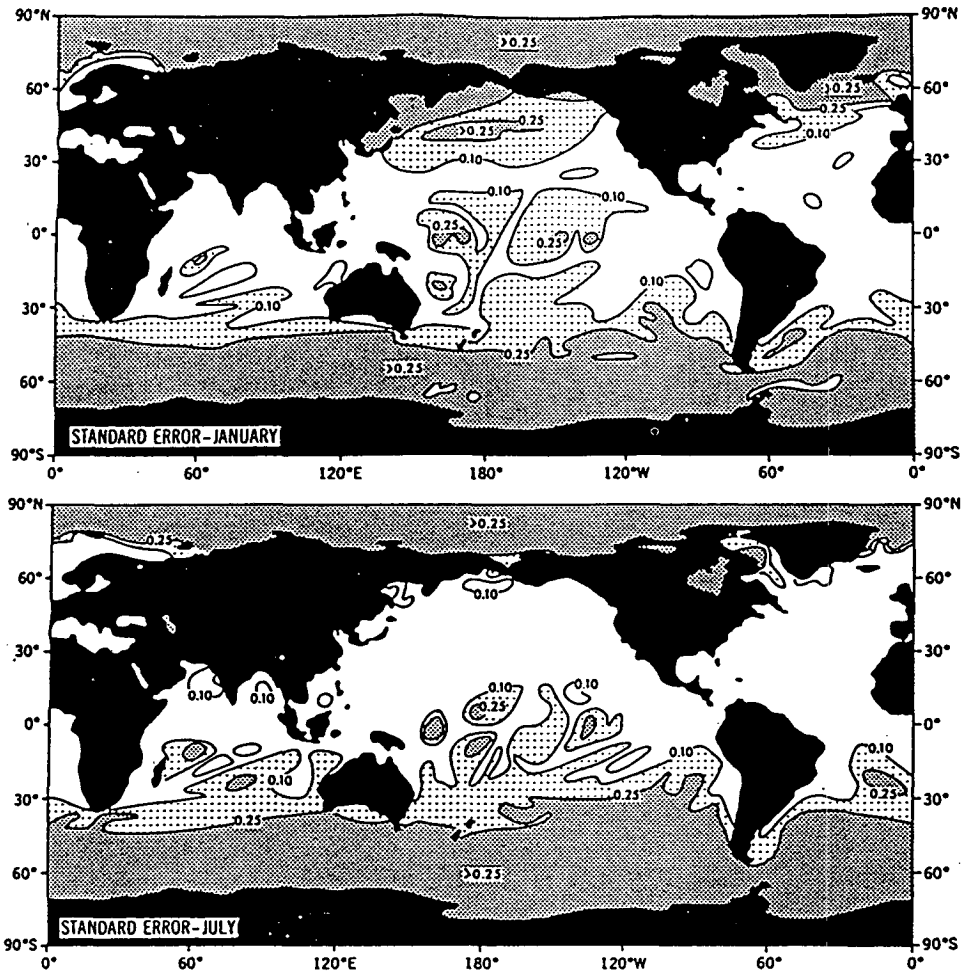

FIG. 1. Standard error of $\tau^{(x)}$ (dynes cm^{-2}) for climatological January and June according to H&R formal error estimates. Reproduced from Hellerman & Rosenstein's (1983) Fig. 5. Note that 1 (dyne cm^{-2}) = 0.1 (Newton m^{-2}).

convert surface observations into a stress datum and from uncertainty in the drag coefficient. H&R assume that a stress estimate can be obtained from a bulk formula of the form:

$$(\tau^x, \tau^y) = \rho_A C_D(|\mathbf{u}|, T_{\text{air}} - \text{SST})|\mathbf{u}|(u, v) \quad (1.1)$$

where values of drag coefficient, C_D, are given in their Fig. 3. Their error estimates address the uncertainty resulting from averaging individual observations using (1.1), and assuming no uncertainty in C_D.

In fact, the dependence of C_D upon windspeed, $|\mathbf{u}|$, and atmospheric stability (which is controlled by more than simply the air–sea temperature difference) remains uncertain. Recent efforts to determine the dependence of C_D upon windspeed, at neutral atmospheric stability, suggest that both the form and the values used by Hellerman and Rosenstein (1983) should be altered. Although there is general agreement that the Hellerman and Rosenstein C_D values can be improved, the exact adjustment remains uncertain at perhaps the 10% to 20% level. The neutral stability form preferred by Large and Pond (1981) and its plausible uncertainty is shown in Fig. 1 of Harrison (1984); Smith [1981, 1985 (personal communication)] has indicated that his preferred form would lie within the uncertainty limits given there. The dependence of C_D upon the atmospheric stability parameter is given through the forms presented in Large and Pond (1981). It is important to note the caveats offered by e.g., Large and Pond (1981), concerning use of a bulk formula; in changing conditions surface stress may depend upon more than simply atmospheric stability and wind speed, so that a bulk formula estimate can be substantially in error. Over time, one can only hope that such errors will tend to average out.

Clearly, uncertainty in estimates of climatological stress must include the effect of drag coefficient uncertainty. This paper describes a first effort to do that, by presenting new climatological monthly mean stresses based upon a surface dataset similar to that used by

H&R, but using the drag coefficient formulation of Large and Pond (1981). It will become clear, through comparison of these results with those of H&R, that the differences resulting from use of this C_D formulation generally significantly exceed the uncertainty estimates of H&R.

In section 2, the method of estimation of sea surface stress is described, as is the dataset upon which these estimates are based. In section 3, sample stress results are presented and compared with results from H&R. Section 4 concerns estimates of wind stress curl fields. Finally, the implications of these results are discussed in section 5.

2. How the stress estimates were made

Following Large and Pond (1981), given a set of surface and near-surface data, the bulk formula

$$\tau = (\tau^x, \tau^y) = \rho_A C_D(|\mathbf{u}|, Z/L)|\mathbf{u}|(u, v) \quad (2.1)$$

was used to estimate the surface wind stress vector τ in terms of the speed, $|\mathbf{u}|$, of the vector wind $\mathbf{u} = (u, v)$, assumed to be known at a height of 10 m above the sea surface, and the atmospheric stability parameter, Z/L, which is assumed to depend upon air temperature (also assumed to be at 10 m height), sea surface temperature, relative humidity and wind stress; ρ_A was taken to be 1.2×10^{-3} g cm^{-3}. The neutral stability form of C_D at 10 m with wind speed was taken to be

$$C_{D10}^N = \begin{cases} 1.15 & \text{for } |\mathbf{u}| < 11 \text{ m s}^{-1} \\ 0.49 + 0.065 * |\mathbf{u}| & \text{for } |\mathbf{u}| > 11 \text{ m s}^{-1}. \end{cases} \quad (2.2)$$

Evaluation of the stability parameter is done through the iterative process described by Large and Pond (1981). It is important to note that a small air–sea temperature difference does not necessarily imply conditions close to neutral stability.

Data were taken from the "HSST" dataset of the National Climate Data Center. Basically, the HSST dataset is a stripped-down form of the full marine surface deck (TDF-11), that includes air and sea temperatures, wind, location, and time. Data from 1850 through 1979 were used in the Atlantic and Indian oceans, while only data between 1950 and 1979 were used in the Pacific.

The later data period was used so that the tropical Pacific climatology be comparable with that of Wyrtki and Meyers (1976). The interannual variability of conditions in the tropical Pacific is large and, together with the limited sampling of this vast area, combines to produce substantial decade-to-decade changes in monthly "climatological" means. The problem of selecting the most appropriate long-term average "climatology" of the Pacific thus requires a special effort; this is not the purpose of the work described herein.

Because the HSST data do not include relative humidity values, it was necessary to decide how to deal with the specification of humidity, in order to make stability calculations. After various experiments, it became clear that changes in relative humidity between 0.85% and 0.25% contributed to drag coefficient uncertainty of at most a few percent, except for wind speeds below $\sim$3 m s^{-1}. It was thus decided to assume relative humidity of 0.70 for all calculations.

In general, the drag coefficient values obtained in this study are smaller by $\sim$20% than those of H&R. This result was expected, based on the tables of Smith (1981), upon inserting typical air–sea parameters. At low windspeeds, where the Large and Pond (1981) neutral coefficient is subject to more uncertainty, their C_D values can exceed those of H&R.

3. Climatological monthly mean stresses

Figure 2 presents, on a 2° grid, the annual mean zonal and meridional wind stress components from this calculation, smoothed by a running 2° lat by 10° long average and then further smoothed by a five point nearest neighbor average. This much smoothing is necessary for clarity of presentation at the reduced scale required in journal publication; note that small-scale spatial structure remains south of $\sim$30°S within $\sim$40° of long of South America and north of 50°N off of the North America coast. These regions of considerable variance are not well sampled. Apart from these areas, the large-scale surface features, well known from earlier studies, are clear.

Figure 2 also shows the gross differences of stress between this calculation and that of H&R. Large-scale zonal stress differences in excess of 0.2 dynes cm^{-2}, are found over much of the trade wind areas, near the Gulf Stream and Kuroshio separation regions and in the area of maximum northern hemisphere westerlies. In all cases, the H&R stresses are larger than the new results. As a fraction of the mean zonal stress, 0.2 dyn cm^{-2} represents 25%–30% in the trades and 20%–30% in the westerlies. Note that these differences substantially exceed the formal error estimates of H&R. Meridional annual mean stress differences are typically less than 0.2 dyn cm^{-2}; only near continental margins and in poorly sampled areas are differences this large found.

Now consider briefly the differences in individual climatological monthly means. Figure 3 presents τ^x and τ^y fields for this calculation and from H&R for climatological January. First consider the zonal stress (Fig. 3a and 3b). Except north of 55°N, there is extremely good pattern similarity between the two calculations. Magnitude differences are nontrivial, however: H&R has >1.4 dyn cm^{-2} maximum stress in the North Atlantic NE trades, while this calculation just exceeds 1.0 dyn cm^{-2}; they have >1.2 dyn cm^{-2} maximum stress in the Indian Ocean SE trades, while this calculation

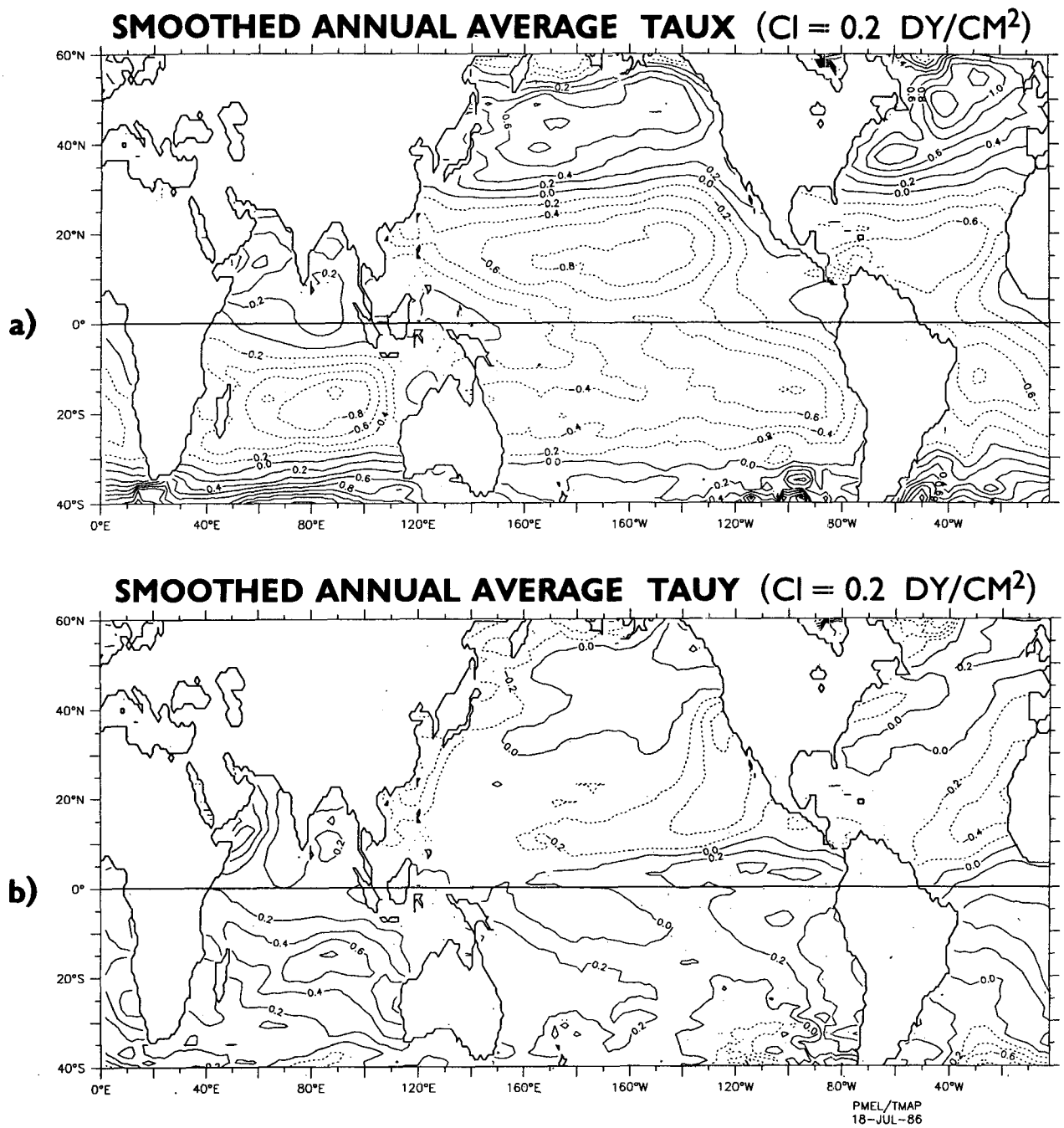

FIG. 2. Climatological annual average wind stress: (a) smoothed $\tau^{(x)}$, this calculation; (b) smoothed $\tau^{(y)}$, this calculation; (c) difference between (a) and HR $\tau^{(x)}$; (d) difference between (b) and HR $\tau^{(y)}$.

just exceeds 0.8 dynes cm^{-2}, etc. Across the core of the trades, differences >0.2 dyn cm^{-2} are common. In the vicinity of the Gulf Stream and Kuroshio, the stress maxima are only different by about 0.2 dynes cm^{-2} (or 10% of the mean stress), but the gradients of stress are so large that differences of detail can lead to stress differences of >0.4 dyn cm^{-2} in the Atlantic and 0.8 dyn cm^{-2} in the Pacific.

The January meridional wind stress fields also show some substantial differences (Fig. 3c, 3d). Near the equator at 120°W, the H&R stress is ~50% greater; the maximum off the southwestern part of Africa is

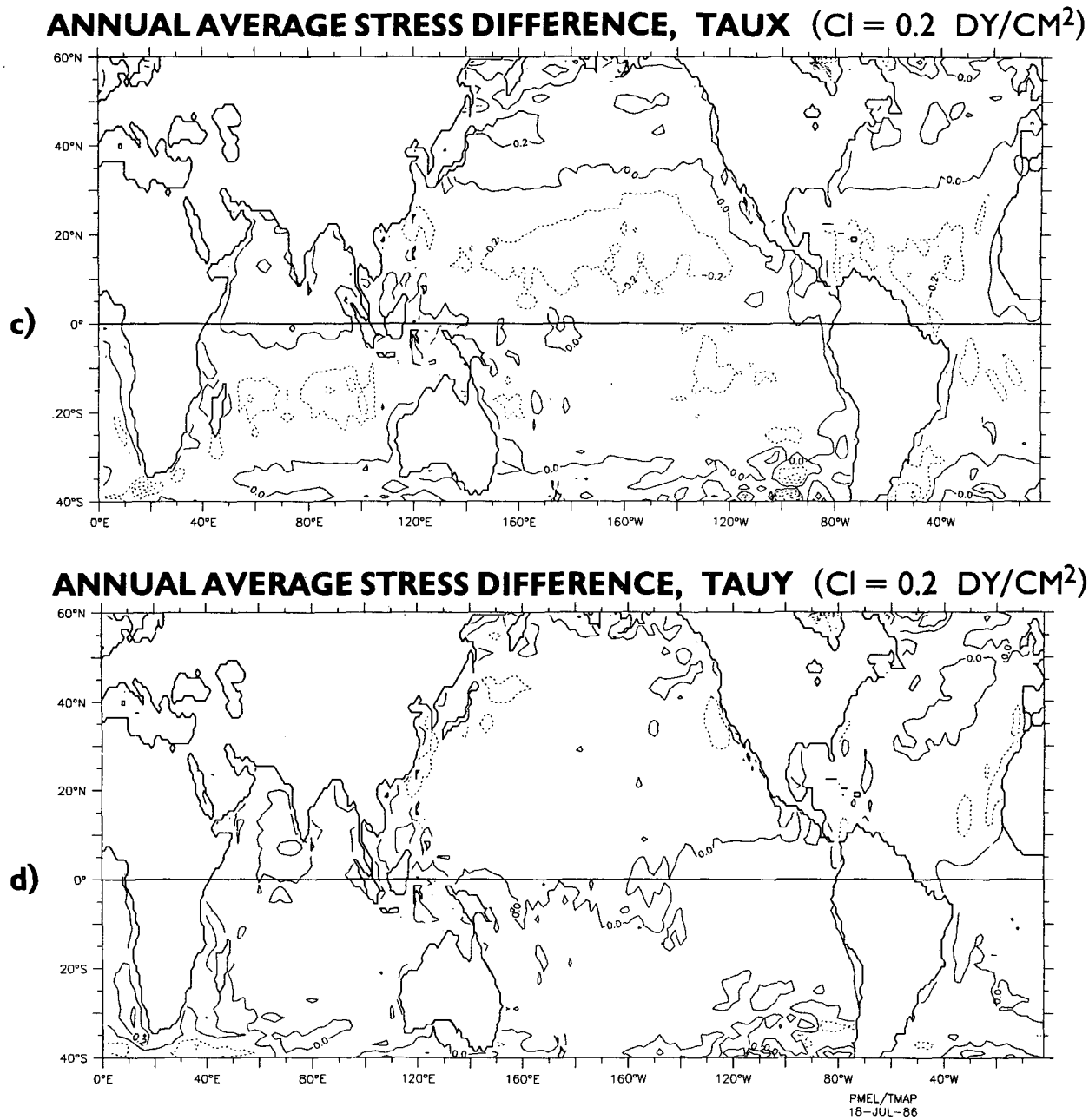

FIG. 2. (*Continued*)

~40% greater; see also the eastern North Pacific and North Atlantic north of ~50°N and the Asian monsoon area. However, the pattern similarity remains strong over most of the world ocean.

Figure 4 presents stress components for climatological July. For the zonal stress (Figs. 4a and 4b), the largest differences in pattern are found in the Southern Hemisphere, south of ~35°S; the roaring forties and more southern latitudes are clearly poorly sampled in Austral winter. Otherwise, patterns are very similar. Difference magnitudes are now familiar—again, H&R values are larger by >0.2 dyn cm^{-2} over much of the tradewind areas. Other regions of substantial zonal stress difference are off the northwestern United States coast and in the Arabian Sea.

The meridional stress fields (Fig. 4c, 4d) are much noisier in the Southern Hemisphere than before, even with the considerable smoothing that has been applied

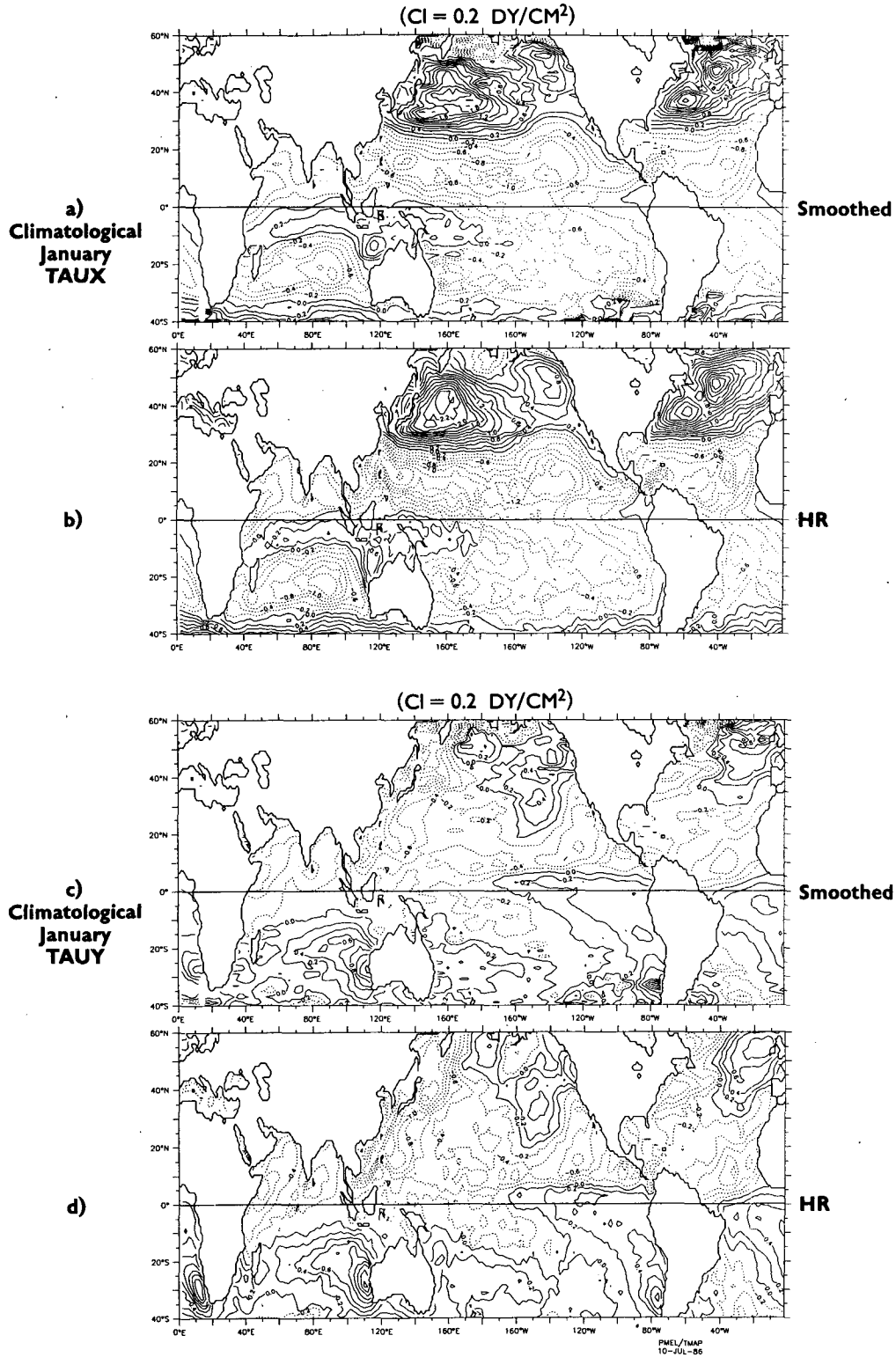

FIG. 3. Climatological January wind stress: (a) $\tau^{(x)}$, (b) $\tau^{(y)}$, (c) $\tau^{(x)}$ HR, and (d) $\tau^{(y)}$ HR.

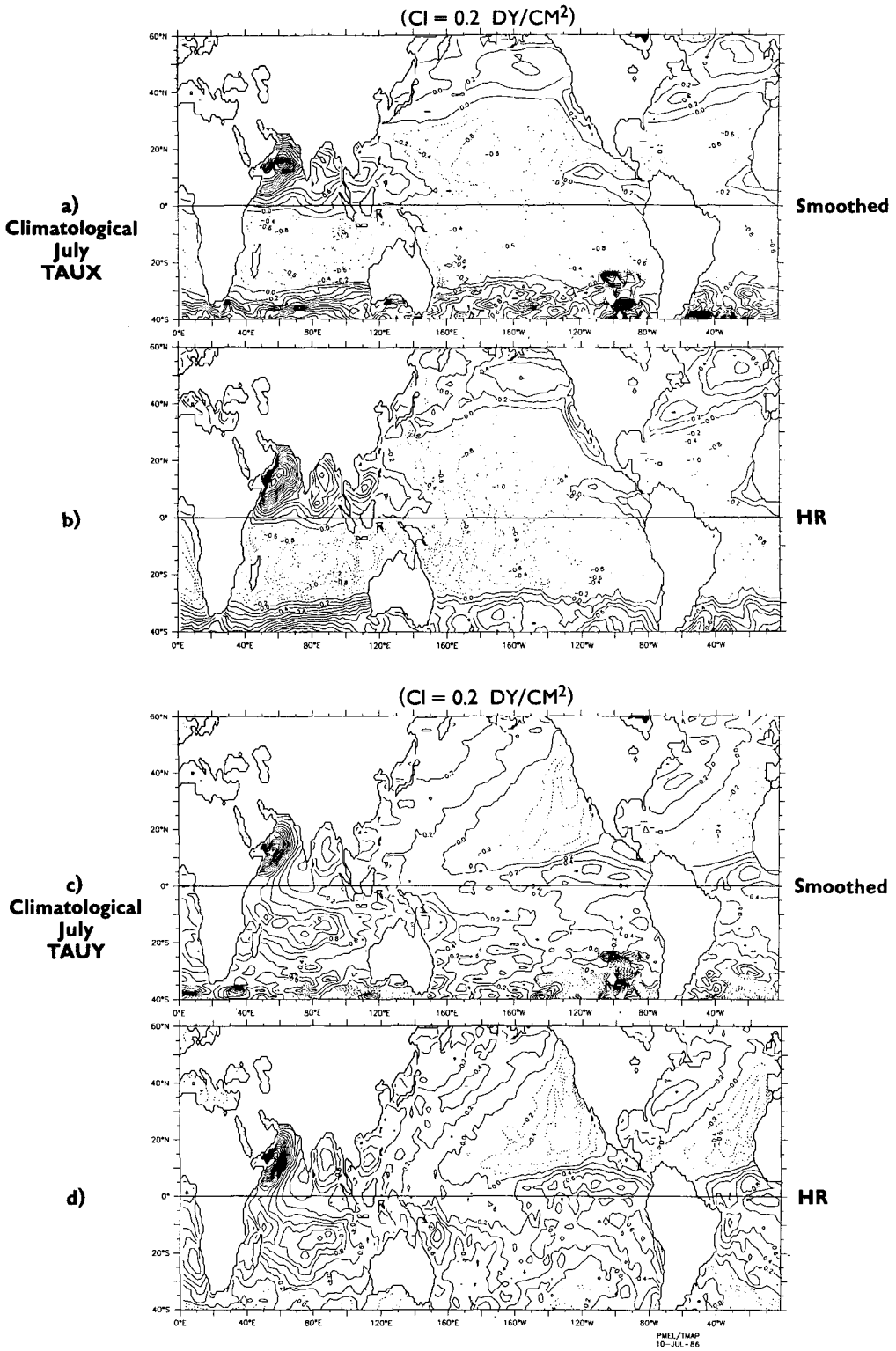

FIG. 4. As in Fig. 3, except for July.

to each field. The largest differences of significant spatial scale are off of the northwestern United States and African coasts and in the East African monsoon area.

A simple measure of the large-scale consequence of these differences is the meridional Ekman transport as a function of latitude, integrated across each basin (Table 1). Except in the South Pacific poleward of ~30°S, the signs agree well, but the quantitative differences can be substantial. At 15°N, H&R Pacific and Atlantic transports are 34 and 17 Sv (Sv ≡ 10^6 m^3 s^{-1}), respectively, while the new values are 26 and 13 Sv, respectively; these differences increase equatorward and decrease poleward. Fortunately, at ~25°N there is little annual mean Ekman transport according to either analysis, so studies like that of Hall and Bryden (1982) would be affected relatively little by these differences.

4. Wind stress curl estimates

The curl of the wind stress, $\text{curl}_z\boldsymbol{\tau} = \dfrac{\partial \tau^y}{\partial x} \Big/ \dfrac{\partial \tau^x}{\partial y}$, is a major forcing component of the vertically integrated mass transport of the mean ocean circulation. Clearly, if two stress analyses differed only by a constant amount, the curls would differ by the same amount. However, we noted both systematic differences in the stress fields over large areas, and differences with considerable spatial structure, especially near some coasts. As these would suggest, curl differences can be considerable.

Figure 5 shows the annual average curl fields from a smoothed version of this analysis and from the H&R analysis. In the trade wind regions, H&R curl values are typically 20% to 50% greater than these values but spatial patterns are very similar. Midlatitude offsets are typically ~20%, but substantial spatial differences are found in the Northern Hemisphere, where the Gulf Stream and Kuroshio leave their coasts, off the west coast of the United States, and off the Strait of Gibraltar. The most dramatic Southern Hemisphere differences occur in the data-poor regions south of ~30°S.

The Gulf Stream separation region difference deserves particular note, as this analysis indicates that the region of positive curl into which the stream passes, has maximum value of $\sim 10^{-8}$ dyn cm^{-3} while the H&R region has maximum value of $\sim 6 \times 10^{-9}$ dyn cm^{-3}. Because the separation physics of western boundary currents involves a delicate balance of forcing, inertial and frictional effects, this difference may help explain why it has been so difficult to get realistic boundary current separation in ocean circulation model simulations. This will be discussed further in section 5.

The annual variation of curl is known to force large seasonal changes in parts of the tropics, particularly in the Pacific and Atlantic north equatorial countercurrents (NECC). Figure 6 shows January and July curl

TABLE 1. Integrated meridional Ekman transport in sverdrups (10^6 m^3 s^{-1}).

Latitude (°)	Indian		Pacific		Atlantic	
	New*	H&R+	New	H&R	New	H&R
59			0.7	0.2	−1.4	−1.7
57			0.1	−0.3	−2.3	−2.4
55			−0.6	−1.2	−2.5	−2.9
53			−1.8	−2.3	−2.6	−3.1
51			−2.5	−3.5	−3.1	−3.6
49			−3.4	−4.6	−3.2	−3.8
47			−4.2	−5.5	−3.3	−4.0
45			−4.6	−6.1	−3.4	−4.1
43			−4.4	−6.3	−3.0	−3.8
41			−4.6	−6.3	−3.0	−3.9
39			−4.6	−6.1	−3.3	−3.8
37			−4.3	−5.5	−3.6	−3.9
35			−4.5	−4.9	−3.0	−3.1
33			−4.5	−4.0	−2.0	−2.0
31			−2.8	−1.6	−0.7	−0.5
29	0.0		0.1	3.4	1.1	2.2
27	−0.2		3.7	6.3	2.8	4.2
25	−0.1	−0.6	7.3	10.4	4.9	6.6
23	−0.6	−0.9	11.0	15.0	6.3	8.2
21	−0.9	−1.6	15.9	21.0	7.9	10.2
19	−2.1	−2.4	19.6	26.0	8.9	11.6
17	−3.1	−3.4	22.6	29.4	11.6	14.8
15	−4.2	−4.9	26.1	33.9	13.1	16.8
13	−5.5	−4.7	28.6	38.3	14.4	18.3
11	−3.8	−5.7	30.6	41.4	11.1	14.2
9	−7.4	−7.3	32.6	42.0	9.2	11.8
7	−11.8	−9.4	32.9	43.0	8.2	11.0
5	−14.3	−12.2	37.9	48.9	7.9	10.6
3	−18.8	−17.1	55.2	71.9	12.9	17.4
−3	0.8	1.3	−68.9	−84.6	−25.0	−31.8
−5	−6.0	−7.5	−47.2	−55.6	−13.3	−17.1
−7	−9.9	−12.3	−34.3	−42.5	−11.7	−14.6
−9	−13.7	−17.1	−28.7	−35.9	−10.7	−13.3
−11	−14.1	−19.5	−26.3	−32.7	−9.9	−12.5
−13	−13.2	−18.5	−23.3	−29.9	−8.9	−10.9
−15	−17.4	−17.6	−21.5	−26.6	−7.8	−9.6
−17	−16.8	−15.7	−18.4	−23.0	−6.7	−8.2
−19	−11.3	−13.7	−16.6	−19.8	−5.5	−6.9
−21	−9.5	−11.7	−13.7	−16.2	−4.6	−5.8
−23	−8.1	−9.7	−10.1	−12.4	−3.7	−4.8
−25	−7.0	−8.3	−8.7	−9.2	−2.9	−4.0
−27	−5.2	−6.1	−4.7	−6.3	−2.1	−2.9
−29	−2.1	−3.3	−5.9	−3.5	−0.7	−1.6
−31	0.3	−0.2	−6.6	−0.6	1.1	0.4
−33	1.2	2.8	−0.9	1.7	2.5	2.0
−35	6.4	6.4	−3.1	3.1	3.9	3.4
−37	9.6	8.9	−6.5	4.3	5.7	4.9
−39	12.1	12.0	−4.2	5.5	7.2	6.2
−41	14.6	14.4	−3.9	7.0	8.0	7.8
−43	15.8	15.4	0.5	7.9	8.0	8.0
−45	14.4	15.0	2.3	8.8	7.9	7.9
−47	14.8	13.5	5.4	10.0	8.3	7.4
−49	9.1	11.5	2.2	10.5	4.6	6.7
−51	9.0	9.4	2.4	10.2	5.5	5.4
−53	10.8	7.7	−3.2	9.4	4.8	5.4
−55	8.4	6.0	1.8	8.6	3.5	4.3
−57	5.2	4.6	−1.5	7.5	1.6	3.6
−59	−1.6	3.3	−5.3	6.2	−0.1	2.8

* New refers to study described herein.
+ Hellerman and Rosenstein (1983).

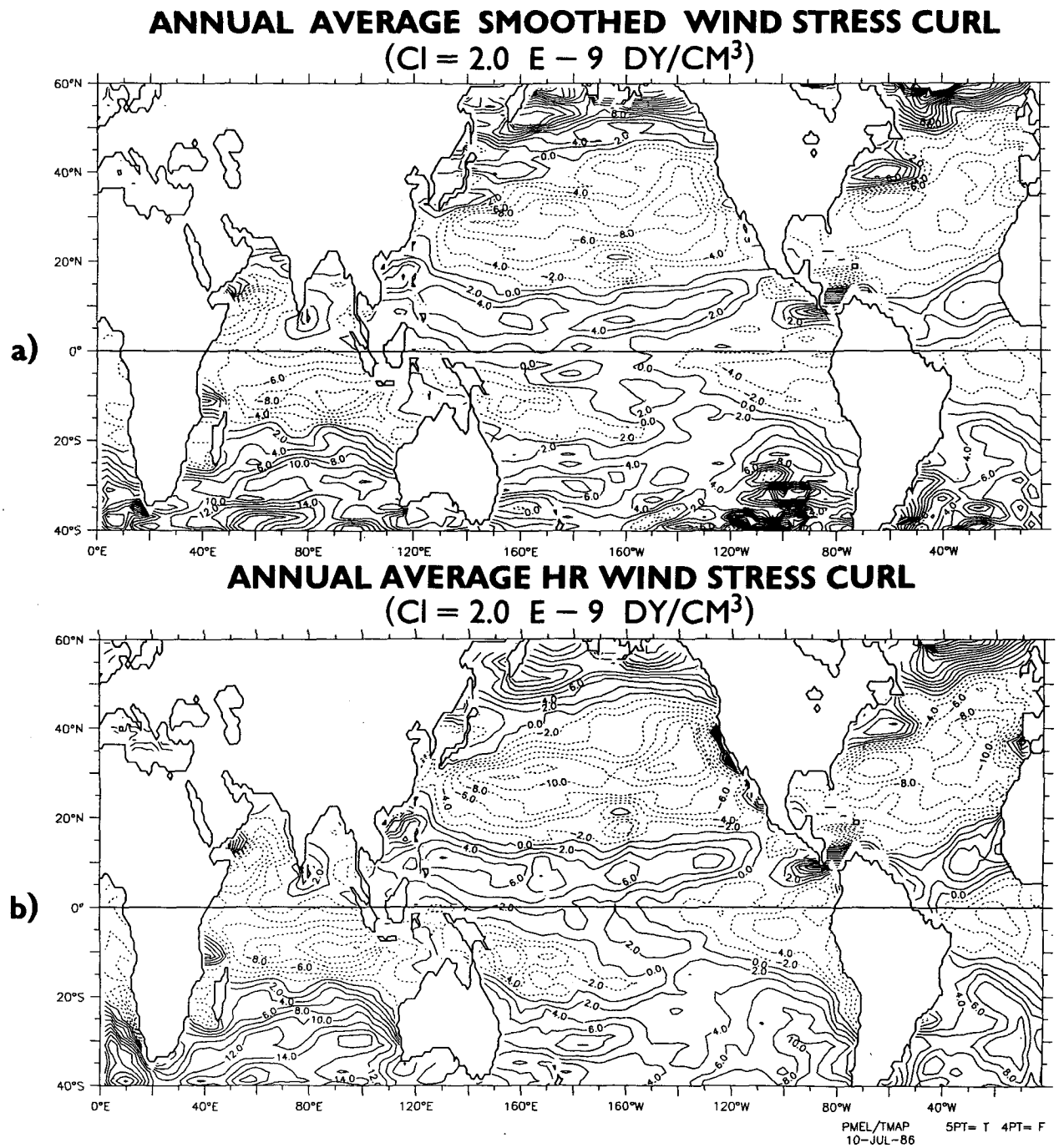

FIG. 5. Annual average wind stress curl: (a) this calculation, and (b) HR. Note that 1 dyn cm^{-3} = 10 N m^{-3}.

fields from this analysis and from H&R. The large movements of the band of positive curl, between ~15°N and somewhat south of the equator, are clear in each analysis. Less evident at first glance, are comparably large changes in the central and western South Pacific between ~15°S and the equator; these curl changes are associated with movement of the South Pacific convergence zone. The tremendous curl changes in the western Indian Ocean, associated with its monsoonal regime, are also clear. These features have been discussed in previous studies.

Less discussion has been given in the literature to the annual curl changes in Northern Hemisphere middle latitudes. In the Gulf Stream separation region, the

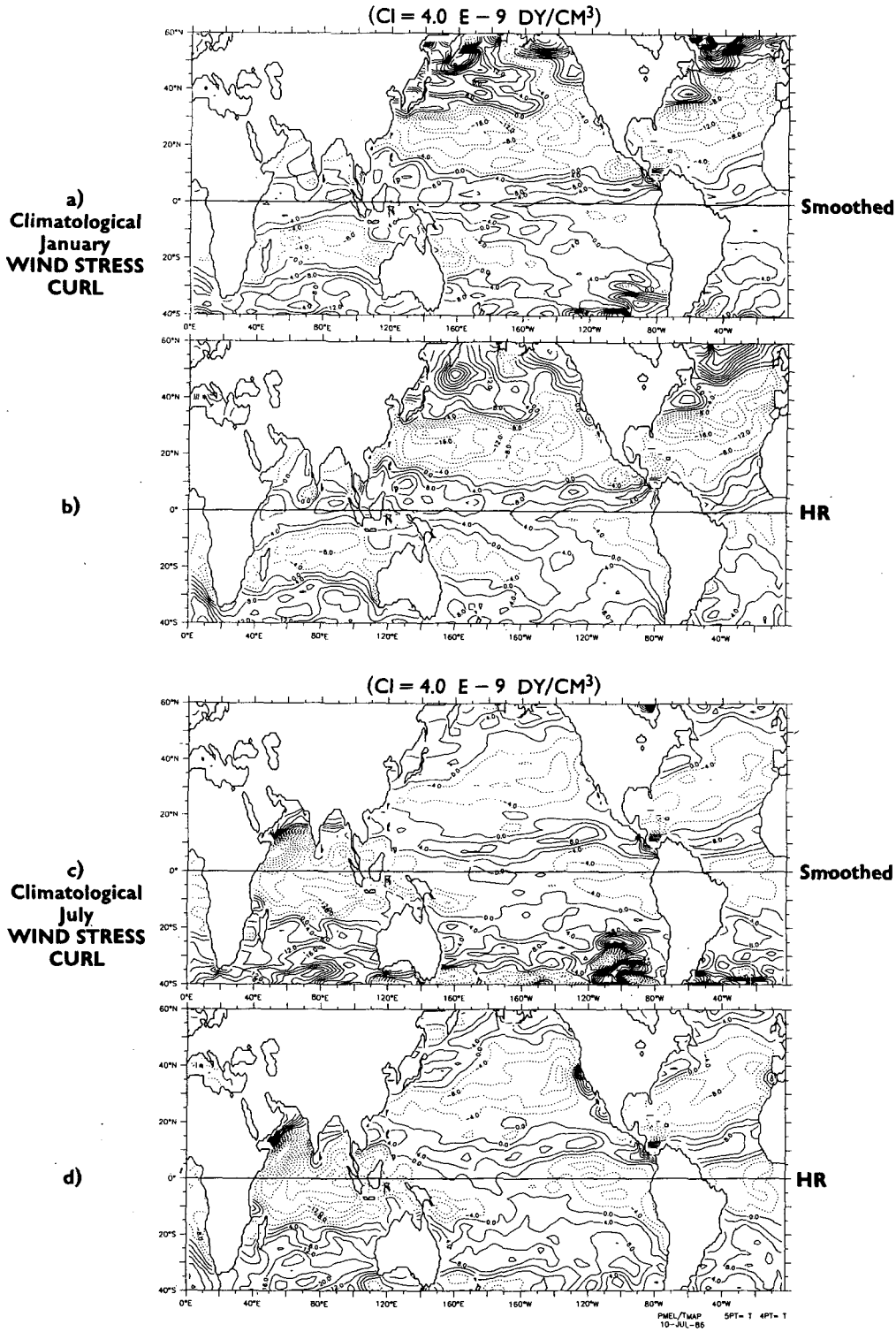

FIG. 6. January wind stress curl: (a) this calculation, and (b) HR. July wind stress curl: (c) this calculation, and (d) HR.

negative curl extremum varies from $\sim 2.4 \times 10^{-8}$ dyn cm^{-3} in January to $\sim 0.8 \times 10^{-8}$ dyn cm^{-3} in July; in the comparable part of the Pacific, the change is between ~ 2.4 and 0.4 ($\times 10^{-8}$) dyn cm^{-3}. For comparison, at 7°N, 130°W the variation is between 0.8 and -0.4 ($\times 10^{-8}$) dyn cm^{-3}. By this very simple measure, the boundary current separation regions experience roughly a 50% greater annual local change in curl forcing than the Pacific NECC in mid-ocean.

South of ~ 30°S the two analyses differ greatly in magnitude and significantly in pattern. In the Pacific in wintertime there are few observations in this analysis, so the features off South America are most likely artifacts of the very limited amount of data there. However, the large differences with Atlantic and Indian Oceans, where data beginning in 1850 are used, suggest that our knowledge of the curl is poor at these latitudes.

One simple way to summarize the large scale differences in these curl fields is by comparing the predicted Sverdrup transport distributions. As is traditional, transport stream function is taken to be zero on the eastern side of each ocean, so the Sverdrup transport is evaluated from

$$\psi_s = \frac{1}{\beta} \int_{x_E}^{x_W} \mathrm{curl}_z \tau dx. \quad \text{(volume transport)}$$

The annual average ψ_s fields are shown in Fig. 7, evaluated from the smoothed analysis and from H&R. Patterns are very similar, except in the Gulf Stream separation region, east of Australia, and in the southern Atlantic, and magnitudes are often quite similar. Transport through the Florida Straits is about 30 Sv according to H&R and about 25 Sv according to this study; off the southern tip of Japan, the transport is ~ 50 Sv, according to both this study and H&R.

Although the Sverdrup transport for individual months does not necessarily give an indication of the time monthly variability of transport, it provides an index for the annual changes in curl. January and July Sverdrup transport fields are shown in Figure 8. According to this analysis, the change in transport in the Florida Strait is between ~ 35 and ~ 20 Sv, while the change at the southern edge of Japan is between ~ 80 and ~ 40 Sv. The comparable H&R values are ~ 40 and ~ 30, Sv and ~ 90 and ~ 40 Sv. Many differences of detail are evident in Fig. 8, particularly in the Southern Hemisphere, south of ~ 20°S.

5. Discussion

The preceding results, based on comparison of new global climatological stress fields, derived using Large and Pond (1981) drag coefficients, and the Hellerman and Rosenstein (1983) stress fields, derived using drag coefficients due to Bunker (1976), indicate that the formal error estimates on the H&R stress fields understate the actual uncertainty of their monthly climatological stress fields. Over much of the ocean, H&R stresses are larger than the new values by ≥ 0.2 dyn cm^{-2}, while H&R error estimates for their stresses are generally less than 0.1 dyn cm^{-2}. The actual stress differences between the two climatologies often vary significantly with geographical location and time of the year. Data limitations south of 20°–30°S lead to very large differences in this region.

Although the large-scale patterns of wind stress are quite similar, there are sufficient differences to cause significant wind stress curl differences in some areas where data coverage is good. In particular, the regions of Gulf Stream and Kuroshio separation show very interesting differences. In the Atlantic, the area of positive wind stress curl that is adjacent to the Gulf Stream is significantly more intense than in the H&R results; if it is correct that the H&R results underestimate the magnitude of this feature, this may account for some of the difficulty that ocean modelers have experienced in getting model Gulf Stream separation to occur at realistic latitudes (Cox, personal communication, and Holland 1986, personal communication).

This result underscores the fact that most midlatitude ocean circulation theory and modeling in basins has been done with imposed wind stress curl fields that bear very little resemblance to North Atlantic climatological curl patterns; it seems worthwhile to repeat some of the previous studies with more realistic patterns. For such purposes, the following zonal stress function,

$$\tau^x = 0.6 \sin\left[\left(\frac{\theta - 30}{25}\right)\pi\right] + 0.4 \exp\left[-\left(\frac{\theta - 38}{5}\right)^2\right] \exp\left[-\left(\frac{\lambda - 60}{10}\right)^2\right],$$

for

$$\theta \in (15, 45) \text{ latitude}$$

$$\lambda \in (20, 80) \text{ longitude}$$

is a usefully more realistic forcing function for this latitude-longitude area, but will produce Ekman suction and pumping distributions that do not permit mass to be conserved strictly within the region; the need for a multi-gyre analysis is evident.

This entire discussion has been based on a heavily spatially smoothed version of the new wind stress climatology. The basic calculation treated all data within 1° latitude-longitude squares as representative of the center of this "grid box," and has a great deal more spatial structure than is suggested by the figures shown here. Much of the structure likely arises from the relatively limited amounts of data available in each grid box, but there is sufficient systematic pattern in data-rich areas to suggest that spatial stress gradients can be much stronger and more spatially confined than is in-

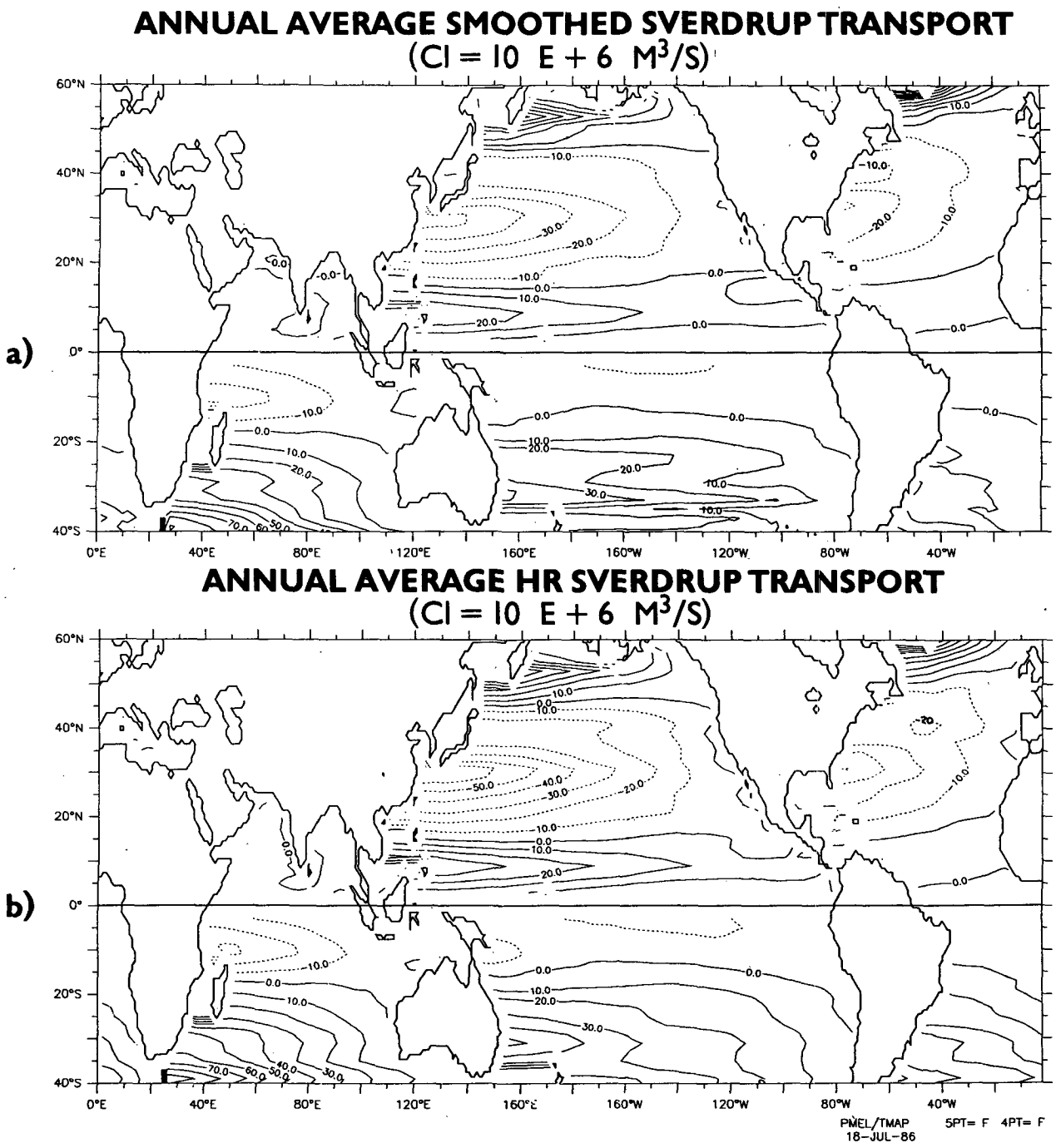

FIG. 7. Annual average Sverdrup transport: (a) this calculation, and (b) HR.

dicated by the figures; this is particularly true near continents and regions of strong SST gradient. No brief discussion can begin to discuss such small-scale stress structure, but awareness of its existence is important; regional forcing must be considered on the finest feasible spatial scales. Saunders (1976) has made these points previously; it is important that they be kept in mind.

Another interesting aspect of the climatological stress fields that has received perhaps less attention than it deserves is the large seasonal changes in wind stress curl over the subtropical and subpolar gyres. In section

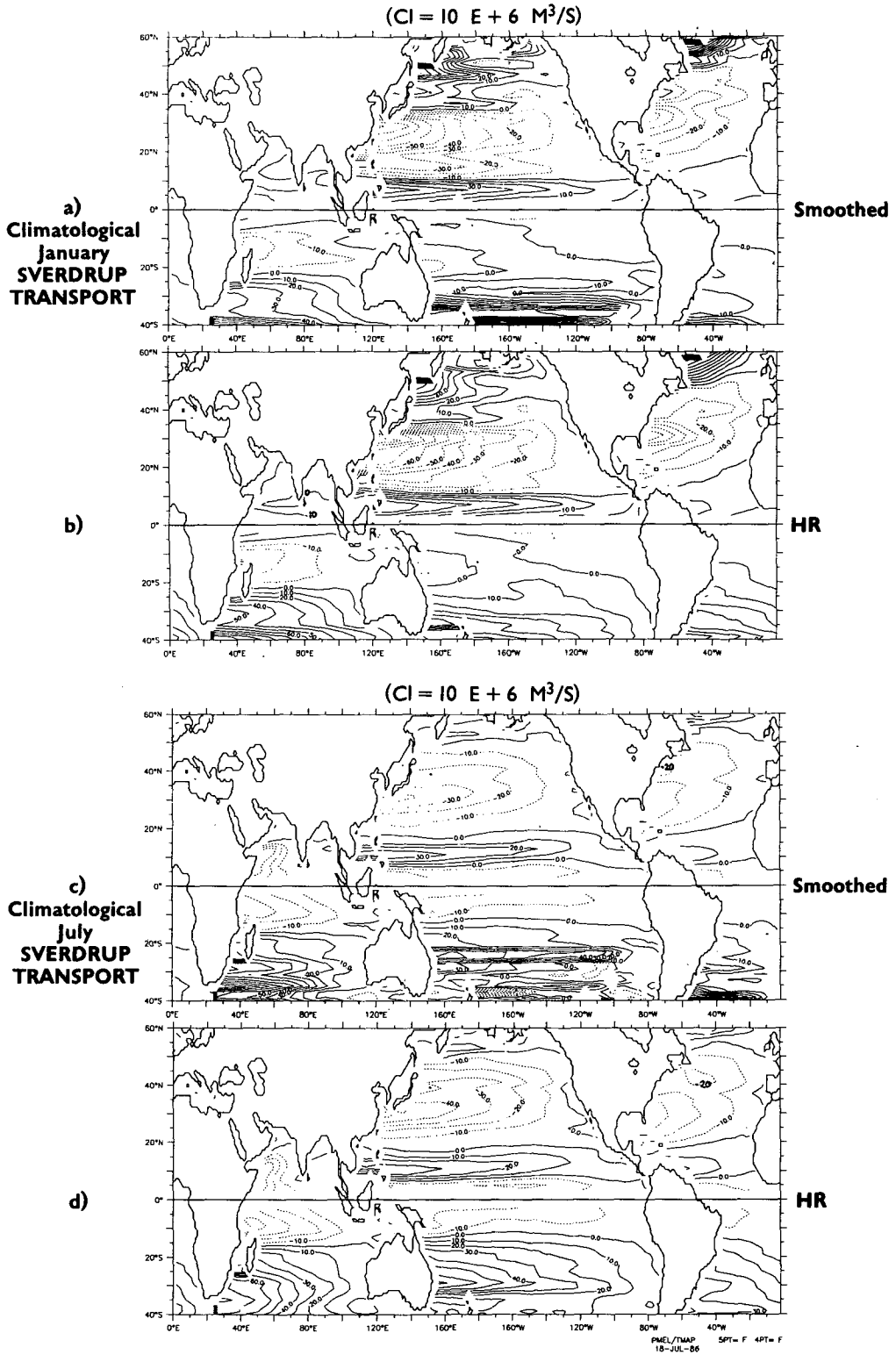

FIG. 8. Sverdrup transport for January, based on January wind stress curl: (a) this calculation, and (b) HR. Sverdrup transport for July, based on July wind stress curl: (c) this calculation, and (d) HR.

4, it was shown that the local annual curl changes in the Kuroshio and Gulf Stream separation regions are roughly 50% greater than those in the Pacific north equatorial counter current. The equilibrium ocean response to such periodic forcing deserves investigation. Recent annual cycle studies by Anderson and Corry (1985) suggest that the very modest annual cycle in Gulf Stream transport observed in the Florida Straits may result from several quite special circumstances; there is no a priori dynamical reason to expect that near-steadiness is characteristic of western boundary current transport. Plans for ocean circulation monitoring for the World Ocean Circulation Experiment cannot afford to neglect a forced annual component of flow.

Although not the subject of this work, other error sources in estimates of the climatological surface wind stress field deserve brief mention. One source is intradecadal variability, which has been found in the ~150 years of surface marine data recently compiled in the NOAA COADS effort. As the data distribution with time is quite uneven through the decades, there may be non-trivial bias in any simple mean. Also, means constructed over a subset of the record may not properly represent the extreme low frequency conditions. Another issue is that there are many ways that individual data errors may not be random, and so formal statistical error estimates may underestimate the true uncertainty. Because of the growing interest in interdecadal climate change, these and other concerns will be receiving much attention in the coming years.

Acknowledgments. Many individuals have assisted in the preparation of this work. M. Halem and J. Shukla provided start-up funding and encouragement at NASA/GSFC; S. Wilson (NASA/Office of Oceanic Processes) and E. Bernard (NOAA/PMEL) provided subsequent support. C. Choquette, S. Stalos, S. Munoz, J. Davison and S. Hankin have provided programming assistance at different stages. Special thanks to W. Large and K. Trenberth for assistance and comments.

REFERENCES

Anderson, D. L. T., and R. A. Corry, 1985: Seasonal transport variations in the Florida Straits: A model study. *J. Phys. Oceanogr.*, **15,** 773–786.

Bunker, A. F., 1976: Computations of surface energy flux and annual air-sea interaction cycles of the North Atlantic ocean. *Mon. Wea. Rev.*, **104.**

Evanson, A., and G. Veronis, 1975: Continuous representation of wind stress and wind stress curl over the world ocean. *J. Mar. Res.*, Suppl. to **33,** 131–144.

Hall, M. M., and H. L. Bryden, 1982: Direct estimates and mechanisms of ocean heat transport. *Deep-Sea Res.*, **29,** 339–360.

Harrison, D. E., 1984: Ocean surface wind stress. *Large-Scale Oceanographic Experiments and Satellites,* Grantier and Fieux, Eds., p. 99–115.

Hastenrath, S., and P. J. Lamb, 1977: *Climatic Atlas of the Tropical Atlantic and Eastern Pacific Oceans.* University of Wisconsin Press.

——, and ——, 1979: *Climatic Atlas of the Indian Ocean Part I: Surface Climate and Atmospheric Circulation.* University of Wisconsin Press.

Hellerman, S., 1967: An updated estimate of the wind stress on the world ocean. *Mon. Wea. Rev.*, **95,** 607–626 (see correction *Mon. Wea. Rev.*, **96,** 63–74).

——, and M. Rosenstein, 1983: Normal monthly windstress over the world ocean with error estimates. *J. Phys. Oceanogr.*, **13,** 1093–1104.

Isemer, H. J., and L. Hasse, 1985: *The Bunker climate atlas of the North Atlantic: I. Observations.* Springer-Verlag, Berlin.

Large, W. G., and S. Pond, 1981: Open ocean momentum flux measurements in moderate to strong winds. *J. Phys. Oceanogr.*, **11,** 324–336.

Leetmaa, A., and A. F. Bunker, 1978: Updated charts of the mean annual wind stress, convergences in the Ekman-Layers and Sverdrup transports in the North Atlantic. *J. Mar. Res.*, **36,** 311–322.

Pedlosky, J., 1979: *Geophysical Fluid Dynamics,* Springer-Verlag, 624 pp.

Saunders, P. M., 1976: On the uncertainty of wind stress curl calculations. *J. Mar. Res.*, **34,** 155–160.

Smith, S. D., 1981: Coefficients for sea-surface wind stress and heat exchange. BI-R-81-19, Bedford Institute of Oceanography, Dartmouth, Nova Scotia.

Veronis, G., 1973: Large Scale ocean circulation. *Adv. in Appl. Mech.*, **13,** 1–92.

——, 1978: Model of world ocean circulation: III. Thermally and wind driven. *J. Mar. Res.*, **36,** 1–44.

Wyrtki, K., and G. Meyers, 1976: The trade wind field over the Pacific Ocean. *J. Appl. Meteor.*, **15,** 698–704.